Journal of Physics: Conference Series **2894** (2024) 012007 doi:10.1088/1742-6596/2894/1/012007

The Role of Polarization for Bound States in Strong Fields

B C Walker, E C Jones, Z Andreula, M R Gale, M Pham, J Wisely
Physics and Astronomy, University of Delaware, 104 The Green, Newark, DE, USA
E-mail: bcwalker@udel.edu

Abstract. As atomic matter interacts with ultrastrong fields, the bound electrons are polarized and have ionization energies changed by Stark-shifting. The unprecedented range of laser intensities from 10^{15} W cm^{-2} to 10^{24} W cm^{-2} can take the interaction from the neutral atom to a bare nucleus. We have used an outer, single active electron approximation to calculate the polarization and Stark-shifted binding energy for ultraintense lasers interacting with highly charged ions at intensities from 10^{14} W cm^{-2} to 10^{22} W cm^{-2}. The polarization of the bound state can result in a dipole moment and Stark shift that may be 0.1 e a_0 and 50 E_h, respectively. At these high intensities, relativistic effects must also be considered. Across the intensity range of these studies, the magnetic field of the laser does not comparably affect the bound state of the atom; the impact of polarization and Stark shift exceed changes to the bound state wave function and binding energy from including relativity.

1. Introduction

Tunneling ionization is fundamental to the physics of attosecond science [1], above-threshold ionization [2], high harmonic generation [3], strong field elastic rescattering of photoelectrons [4], multielectron rescattering ionization [5], and ultra-strong field interactions with highly charged ions [6, 7]. These interactions are often treated in the dipole approximation and ubiquitously use field-free properties for the atom to calculate the ionization rate, neglecting the impact of the strong laser field on the bound state [8]. In Fig. 1, the interaction of a strong field with an atom is shown in the three-step classical model simplification [9]: (1) ionization, (2) acceleration, and (3) recollision. The importance of the current work can be understood in that it addresses step (1) of this sequence and, therefore, influences all subsequent observations.

Additional motivation for this study is the advancement in laser technology. Chirped pulse amplification [10] laser intensities now exceed 10^{23} W cm^{-2} [11], corresponding to electric fields reaching $1,500\ E_h\, e^{-1}\, a_0^{-1}$ in atomic units (Hartree energy E_h, elementary charge e, and bohr distance a_0). At high intensities, the electrons bound to the ions are certainly no longer in a "field-free" environment and the force from the laser magnetic field must be also considered [12]. A Lorentz rescattering parameter [13] was able to differentiate traditional dipole strong-field atomic and molecular interactions and the ultrastrong field regime, where the full laser electric and magnetic field is required to describe the rescattering physics. Larmor radiation [14, 15], bremsstrahlung [16], and high harmonic generation [17] have been studied including relativistic effects. The impact of relativity has also been studied in multielectron interactions with non-sequential ionization [18] and laser recollision inner shell excitation [19]. Recently, an

Content from this work may be used under the terms of the Creative Commons Attribution 4.0 licence. Any further distribution of this work must maintain attribution to the author(s) and the title of the work, journal citation and DOI.
Published under licence by IOP Publishing Ltd

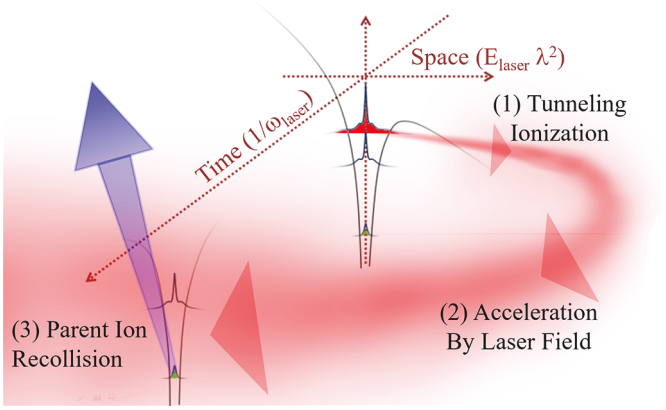

Figure 1. Sequence of (1) tunneling ionization (red) of the outermost electron, (2) laser acceleration of the photoelectron over length scale of E_0 λ^2, (3) electron return on a time scale of $1/\omega$ to the parent ion where recollision occurs (blue).

ultimate energy limit of rescattering [20] was discovered giving an energy maximum for laser-driven rescattering as approximately one thousand Hartree (27 keV).

In this work, we calculate the electron wave function for highly charged ions to characterize the polarization and Stark shift of bound states at intensities generated by modern terawatt [21, 22] and petawatt [23] laser systems. Our findings show an interplay between polarization and the Stark shift resolves how tunneling models based on a 'field-free' approximation can appear to agree with experimental measurements [24, 25, 26, 27, 28, 29] when, in fact, the tunneling rates are impacted by the atomic states polarizing and energy shifting in the external laser field [30].

To introduce how fields change atomic states we briefly examine the response of krypton [27] calculated according to the method described in section II. Theory. In Fig. 2 the outermost electron wave function of Kr^{25+} is shown at an intensity of 1.2×10^{19} W cm^{-2}. The outermost electron is often identified as the spherically-symmetric hydrogenic $3s$, about a closed shell neon $1s^2 2s^2 2p^6$ core. In Fig. 2 one can see the outermost electron wave function $|\psi(x, 0, z)|$ in the plane of the electric field $\vec{E} = 12.4\ E_h\, e^{-1}\, a_0^{-1} \hat{z}$. The force from the external field causes the electron to spatially displace away from the nucleus. Fig. 3 is a plot of $\psi(z)^* \psi(z)$ with no external field and at 1.2×10^{19} W cm^{-2}. The shift of the peak electron probability to $z \approx -0.4\ a_0$ is identifiable in Fig. 3 and evaluates to a similarly large electric dipole $\vec{p} = 0.33$ e $a_0\, \hat{z}$. The binding atomic potential for the outer electron with and without the external field is also plotted in Fig. 3 as a function of the distance from the nucleus along the electric field (z-axis). The Stark shift due to polarized state alignment in the external field can be a sizable fraction of the binding energy since $|\vec{p}| \sim 0.1$ e a_0 and ultrastrong fields are of order 10 to 10^2 $E_h\, e^{-1}\, a_0^{-1}$. In Fig. 3 the Stark shift of the binding energy from -44 E_h to -46 E_h is displayed in the potentials as an offset of the electron wave function probability $\psi(z)^* \psi(z)$.

2. Theory

Our model moves beyond a field free atomic bound state by approximating the atomic response as a 'frozen' ion core with a outermost and least tightly bound single active electron (SAE) interacting with the external field ($\vec{E} \cdot \vec{r} = |\vec{E}| z$), and ion core comprised of the nucleus and the electronic density minus the one active electron. The ion core potential $V_{core}(r)$ is computed via Hartree-Fock with a 6-31G* basis and the external laser field off. The electronic

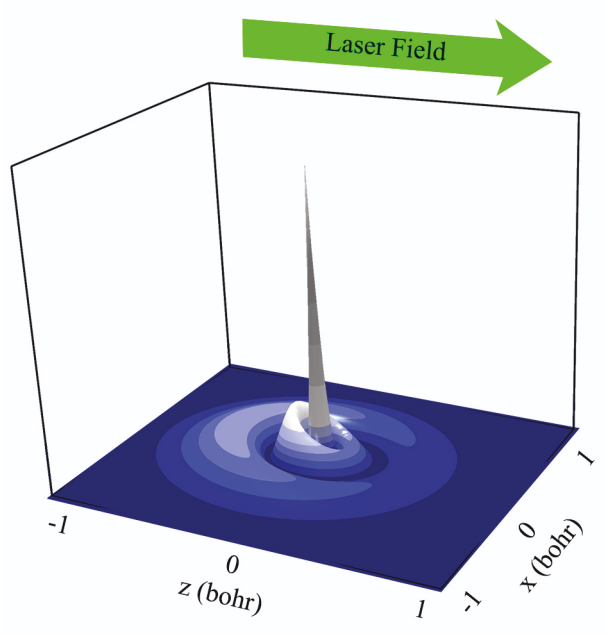

Figure 2. Wave function magnitude $|\psi(x, 0, z)|$ (a) in the $y = 0$ plane for the Kr^{25+} outermost electron in an external electric field (intensity) of 18 $E_h\, e^{-1}\, a_0^{-1}\, \hat{z}$ (1.2×10^{19} W cm^{-2}).

density contributing to $V_{core}(r)$ is in good agreement when compared against Thomas–Fermi, Thomas–Fermi–Dirac, and Dirac–Hartree–Fock–Slater electronic densities from reference [31]. Once $V_{core}(r)$ is obtained, the 3D time-independent Schrödinger equation (TISE) is solved in the quasi-static approximation for SAE in the external field [32]. The TISE in this case takes the following form in atomic units,

$$\left[-\frac{1}{2}\nabla^2 + V_{core}(r) + |\vec{E}|z \right]\psi(\vec{r}) = \epsilon\psi(\vec{r}) \tag{1}$$

where ϵ is the energy eigenvalue, and the external laser field is aligned along the z axis. Eq. 1 is diagonalized with a hydrogenic basis set parameterized with atomic number Z defined by the nuclear charge of the species being calculated. The corresponding matrix elements are calculated to 10^{-6} E_h precision. Convergence of the solution to Eq. 1 is achieved by increasing the size of the basis set to include increasingly large principle quantum number functions along with the corresponding angular momentum quantum number functions. The criteria for basis set convergence is when adding an additional principle quantum number shell changes the SAE energy by less than 10^{-6} E_h with the external laser field on. The polarization and Stark shift energy is then determined from the SAE wave function. The interaction for each species typically ranges from a field strength of 0.1× 'barrier suppression ionization' (BSI), or 'classical ionization,' (0.01 of the BSI intensity) to 0.9×BSI. In this range, the energy and dipole converge with a basis set of typically n=25 for the principal quantum number. The field free ionization energy of the calculated bound states typically ranges within $\sim 10\%$ of NIST values [33].

By way of example and to highlight the relevant energy scales, the calculated ion core potentials, bound states, and radially dependent effective charge for Kr^{25+} are shown in Fig. 4. The core state radial probabilities in Fig. 4(a) are offset in the figure to correspond to the binding energy in the potentials to aid the reader's eye. The electron correlation energy is included in Fig. 4(a) and can be seen to account for up to $\sim 5E_h/e$ of the several hundred Hartree ion core

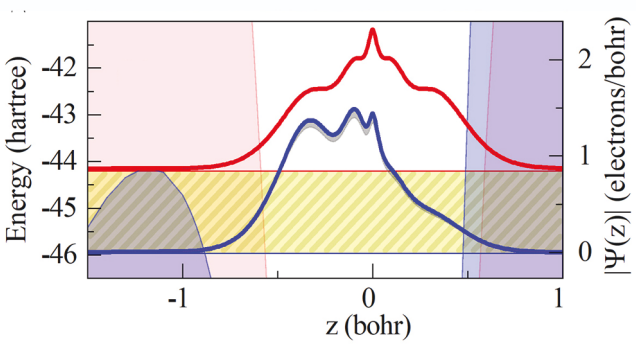

Figure 3. Wave function magnitude for the Kr^{25+} outermost electron in an external electric field (intensity) of 18 $E_h\, e^{-1}\, a_0^{-1}\ \hat{z}$ (1.2×10^{19} W cm^{-2}). The electron probability $\psi(z)^*\psi(z)$ is shown field-free (red, upper bold line) and along the 18 $E_h\, e^{-1}\, a_0^{-1}\ \hat{z}$ field direction (blue, lower bold line). The $\psi(z)^*\psi(z)$ probability (right y-axis) is shown offset to indicate the binding energy of -44.1 E_h field free and -46 E_h in the field. The binding ion potentials for the Kr^{25+} outermost electron ion with no external field (red, thin line, light fill to x-axis) and in an electric field of 18 $E_h\, e^{-1}\, a_0^{-1}\ \hat{z}$ (blue, thin line, dark fill to x-axis) are also shown.

potential that binds the outer electron. For ultraintense laser interactions many electrons are field ionized; the ultraintense field interactions are with highly charged ions. As a result, the large, unscreened nuclear charge dominates the ion core potential. In Fig. 4(a) the bare 36+ nuclear charge (gray, thick line) can be seen to account for most of the ion core potential (red, solid line) with the bulk of the difference between the ion core potential and the bare nuclear potential attributable to the ten-electron shielding. The contribution from electron correlation to the potential is shown in Fig. 4(a) (black, dashed line) as a separated energy term. Fig. 4(b) gives the Kr^{26+} ion core electron radial probability for Kr^{25+}. The localization of ion core to radial values of $r < 0.15\ a_0$ can be compared to the $\sim 0.4\ a_0$ extent of the polarized outer electron wave function. Since polarizability scales as $\sim r^3$, the polarizability of the ion core is neglected as it is typically an order of magnitude less than the polarizability of the outer electron.

3. Polarization and Stark Shift

A detailed analysis of the outermost electron properties for O^{7+}, Kr^{26+}, and Hf^{61+} are presented in this section. The field-free orbital descriptions for these species are O $1s^1$, Kr $1s^2 2s^2 2p^6$, and Hf $1s^2 2s^2 2p^6 3s^1$. These three cases were chosen as they demonstrate characteristic cases of a one-electron atom, active and core electrons in the same shell, and closed-shell ion cores.

The calculated field free binding energy and Stark shifted binding energy of the outermost electron for O^{7+}, Kr^{26+}, and Hf^{61+} are plotted in Fig. 5(a). Depending on the orientation of the electron state, $\vec{p} \cdot \vec{E}$ can increase the ionization energy as the state becomes more tightly bound (more negative binding energies). This is the case for O^{7+} and Hf^{61+} when the induced dipole is parallel to the field. Conversely, the dipole of the outermost electron in Kr^{26+} has an anti-parallel alignment. This lifts the state's energy in the field, decreasing the ionization energy [34]. The magnitude of the outermost electron dipole for O^{7+}, Kr^{26+}, and Hf^{61+} are shown in Fig. 5(b). The alignment of the electron probability $\psi^*(z)\psi(z)$ at an external field 0.71×BSI can be compared to the field-free solution in Fig. 5(c-e).

We begin with O^{7+} at an intensity of 10^{17} W cm^{-2}. The binding energy shifts in the field from -32 E_h to -32.5 E_h, approaching the BSI intensity. The 2.5×10^{-2} e a_0 dipole response at

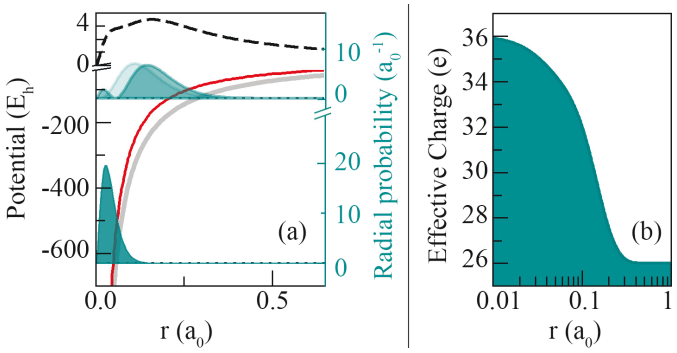

Figure 4. Potential energy (a) for the ion core Kr$[1s^2 2s^2 2p^6]$ (left axis) including the Kr^{36+} nucleus Coulomb potential (gray, thick line), the ion core potential $V_{core}(\vec{r}$ (red, solid line), and electron correlation energy for the core (black, dashed line). A split scale is used in (a) for electron correlation energy. The radial probabilities, right axis of (a), for the electron core states (green fill shading) are offset according to binding energy. The ion core is displayed as the radially dependent effective charge in (b).

one-half of the BSI intensity is barely observable in Fig. 5(c) as a $-0.025\hat{z}\ a_0$ shift of $\psi^*(z)\psi(z)$ from the field free probability.

Turning next to Hf^{61+}, Fig. 5(a) portrays the binding energy changes from the field free value of $-234\ E_h$ to $-262\ E_h$ as one approaches the BSI intensity at 2×10^{21} W cm^{-2}. The induced dipole is of order 10^{-1} e a_0 due to a combination of the larger radial values for the n=3 state and the extremely high intensity. The peak value of $\psi^*(z)\psi(z)$ for the outermost electron in a field strength of $\sim 173\ E_h\, e^{-1}\, a_0^{-1}$ is seen in Fig. 5(e) to be approximately 0.15 a_0 along $-\hat{z}$.

The Stark effect gives a splitting of the energy levels by mixing the atomic states and then interacting with the resulting electric dipole moments. States shifting to lower energies, such as for O^{7+} and Hf^{61+}, result from an alignment with the field. Kr^{26+} illustrates the impact of the external laser field on states shifting to higher energies due to an alignment opposite to the field. In terms of $|nlm\rangle$ states $|200\rangle$, $|210\rangle$, $|21\,{-1}\rangle$, and $|211\rangle$ in an electric field mix to create eigenstates with a dipole moment parallel and anti-parallel to a $\hat{z}$ field: $1/\sqrt{2}\ (|200\rangle - |210\rangle)$ and $1/\sqrt{2}\ (|200\rangle + |210\rangle)$. This high-energy state of the Stark-shifted manifold has its binding energy shifted by $\vec{p}\cdot\vec{E}$ up from the field free value of $-125\ E_h$ to the $-115\ E_h$ shown in Fig. 5(a). The external field forces the electron in the direction of $-\hat{z}$, pushing back the initial alignment along $\hat{z}$; the initial 0.08 e a_0 dipole at 10^{19} W cm^{-2} drops to 0.07 e a_0 as one approaches 10^{21} W cm^{-2}. $\psi^*(z)\psi(z)$ for the outermost Kr^{26+} electron is shown in Fig. 5(d).

Common tunneling models [35] used to calculate the tunneling rates from neutral species and highly charged ions make a single electron approximation for partially filled shells with equivalent electrons. Furthermore, the electrons are treated as degenerate with no consideration for splitting of the n-1 sublevels by the external field. When comparing highly charged ions to neutral species for the same nucleus, highly charged ions have electrons in lower principle quantum numbers. This reduction to low principle quantum number states improves the validity of frozen cores as the binding energy and radial extent change greatly for $n = 1, 2, 3$. One can intuitively justify, for example, the single-active-electron approximation with a frozen closed-shell $n = 1$ core and an outer $n = 2$ electron.

For cases where the ion core and active electron occupy the same shell, such as Kr $2p^6$, including the Stark shift lifts the degeneracy for electrons in the same shell. While not providing the ion-core to active-electron separation that a change in the principle quantum number provides, including the Stark shift significantly lifts the degeneracy of states within the

same shell and improves the justification of treating the electrons separately. By way of example, for Kr $2p^6$, the binding energy of the outer electron is $10E_h$ and $20E_h$ less than the more tightly bound Kr $2p^4$ and Kr $2p^2$ electrons, respectively.

Beyond a frozen core and active outer electron approximation, one may consider the polarizability of the core. For electrons in different principle quantum numbers, the r^3 polarizability scaling highly favors the electrons in the outermost principle quantum number. However, electrons with the same n, l, and $|m_l|$ states will have similar polarizabilities for partially filled shells. Allowing polarization for the core with partially filled shell configurations will effectively decrease the external field experienced by the active outer electron. When compared to a frozen-core model, the partial cancellation of the external field form polarization of the core will reduce, but not eliminate, the polarization and Stark Shift of the least tightly bound active electron.

We have presented results using our numerical solutions to the Schrödinger equation using a hydrogenic basis. To extend the work to other approaches and basis sets, we have used GAUSSIAN 16 [36] with Gaussian basis sets that can account for polarization, such as 6-31 G(d,p) [36]. While commonly used to calculate molecular structure, GAUSSIAN 16 may also be used to calculate atomic orbitals for highly charged ions at the level of Hartree-Fock in ultrastrong external fields. We find the Stark shifts, and induced polarizabilities in external fields calculated using GAUSSIAN 16 are consistent with the results presented. The wide availability of GAUSSIAN 16 means the findings presented here can be incorporated generally for other species or fields with commercially available software.

4. Relativistic Effects

Despite the significant work on relativistic effects in strong laser fields, an 'intuitive model' of relativistic effects for bound atomic states is still lacking. Relativistic effects come into play, for example, as they change the bound state wave function or the interaction with the external field, especially in the spatial region near the tunneling barrier. The changes in the wave function due to relativity and the laser B field effects are small for the interactions considered [7]. For highly charged ion of Ar^{15+}, changes to the field free wave function probability from the E field of order 10% were reported to correspond to changes from the B field of order 0.4%.

There are two additional ways to view the relativity and B field impact. Among the most straightforward is quantifying the force from the external electric and magnetic fields [37]. The work by [37] uses Monte-Carlo trajectory ensembles to give insight into how the laser magnetic field affects the electron in the bound state. Briefly, the forces on the semi-classical electron ensembles as a function of time (given in Kepler Orbits) are studied for ions at field strengths from 0.06 a.u. to 500 a.u. (intensities of 10^{14} W/cm^2 to 10^{21} W/cm^2). Though the role of v/c B relativistic effects increases over this range, they are still 10^4 orders of magnitude smaller than the forces from the electric fields. In terms of 'how quickly' these Lorentz forces impact the dynamics, the scaling can be explained as a function of the highly charged ion binding charge. The increasing influence of the force on the electron at higher intensities due to B_{laser} can be seen from a simple Z scaling. The force from E_{laser} at BSI scales as Z^3 and the corresponding force from B_{laser} scales as Z^4 with the inclusion of the velocity, which scales as Z for the bound-state electron. As a result, one expects relativistic effects (forces and energies) to increase slowly, i.e. approximately linearly, as a function of the ion charge.

The role of relativistic effects and the external laser magnetic field for the bound states of highly charged ions have been examined with semiclassical [37] and quantum [38] treatments. Including the external laser magnetic field in calculations changes the bound state energy by a few percent at 10^{22} W cm^{-2}. For reference, the Zeeman energy from the laser magnetic field acting on the calculated polarized states is given in Fig. 5(a) relative to the Stark shift and bound state energy. For tunneling ionization, the angular distribution of the bound electron

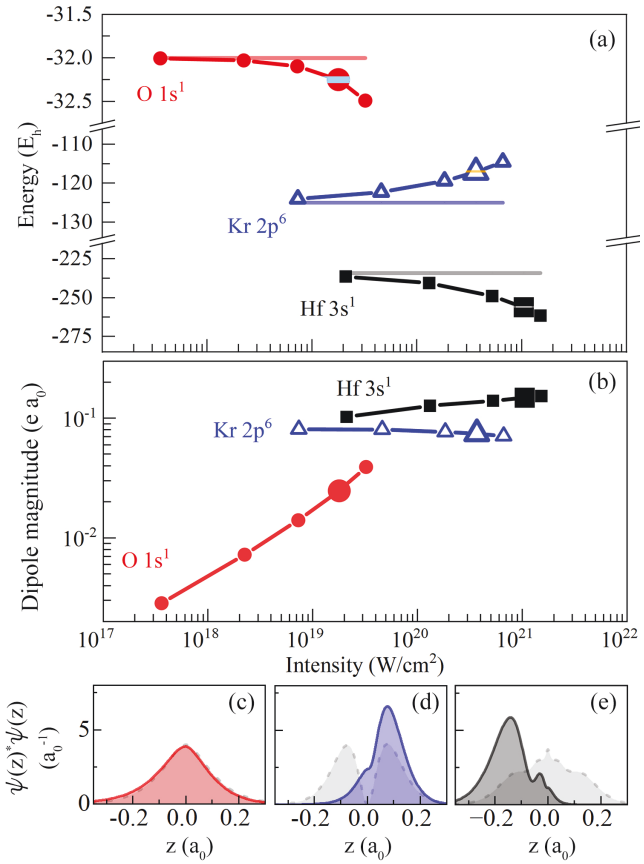

Figure 5. Binding energy (a) for the outermost electron of O^{7+} (red, dark line, filled circle), Kr^{26+} (blue, dark line, open triangle), and Hf $^{61+}$ (black, dark line, filled square) notated by the assignment O $1s^1$, Kr $2p^6$, and Hf $3s^1$, respectively. As an aid to the eye the field free binding energy is indicated as (horizontal, light line) in each case. The dipole magnitude for the outermost electron for O^{7+} (red, filled circle), Kr $^{26+}$ (blue, open triangle), and Hf $^{61+}$ (black, filled square) is shown in (b) as a function of intensity. A larger symbol is used for the 0.71 BSI point, which is the field used in (c-e). $\psi(z)^*\psi(z)$ for the outermost electron are shown for O^{7+} (c) at field of 22.6 $E_h\, e^{-1}\, a_0^{-1}$ (red, solid line, fill); Kr $^{26+}$ (d) at 102.5 $E_h\, e^{-1}\, a_0^{-1}$ (blue, solid line, fill); and Hf $^{61+}$ (e) at 173 $E_h\, e^{-1}\, a_0^{-1}$ (black, solid line, dark fill). The field free $\psi(z)^*\psi(z)$ are also shown in (c-e) for reference (light gray, dash line, light fill). The extent of the Zeeman energy splittings (0.08 E_h for O^{7+}, 0.6 E_h for Kr $^{26+}$, and 1.1 E_h for Hf $^{61+}$ is smaller than the symbol size) are indicated by a highlighted horizontal bar $\Delta\, E_h$ region within the 0.71 BSI Stark shift symbols in (a).

wave function as it appears in the continuum [39] from under the barrier [40] is deflected by ~ 0.1 radian at intensities above 10^{22} W cm^{-2}. This amount is negligible relative to changes in the angular distributions due to the Lorentz force for the photoelectron in the continuum [13]. Despite changes to the angle-resolved photoionization current, the magnetic field does not significantly affect the total ionization rate [37, 41] up to intensities of 10^{22} W cm^{-2}.

The energies for the bound states we consider are $< 2.5\%$ of the electron rest mass. As a result, the relativistic kinetic energy shift and relativistic energy fine structure shift are neglected. Extensions of our work to highly charged ions with intensities above 10^{22} W cm^{-2} [42, 41] will

need to involve careful consideration of the nonrelativistic approximation and role of the external laser magnetic field as well as the linear or circular external field polarization [43].

5. Conclusion

As matter interacts with ultrastrong fields, the bound electrons in ion states are both polarized and Stark shifted. The unprecedented range of laser intensities from 10^{15} W cm^{-2} to 10^{24} W cm^{-2} can take the interaction from the neutral atom to a bare nucleus. We have used a single active electron approximation to calculate the polarization and Stark shifted binding energy of the outermost electron as a function of the external field strength. The calculated response shows induced dipole and Stark shifts as significant as 0.1 e a_0 and 50 E_h. The magnitudes of these changes to the bound states impact common tunneling models that use the field-free approximation for the ionizing bound state [30].

Acknowledgments

This material is based upon work supported by the National Science Foundation under Grant No. 2133728 and 2110462.

References

[1] Chen M C, Mancuso C, Hernandez-Garcia C, Dollar F, Galloway B, Popmintchev D, Huang P C, Walker B, Plaja L, Jaron-Becker A A, Becker A, Murnane M M, Kapteyn H C and Popmintchev T 2014 *PROCEEDINGS OF THE NATIONAL ACADEMY OF SCIENCES OF THE UNITED STATES OF AMERICA* **111** E2361–E2367 ISSN 0027-8424

[2] Yang B, Schafer K, Walker B, Kulander K, Agostini P and DiMauro L 1993 *PHYSICAL REVIEW LETTERS* **71** 3770–3773 ISSN 0031-9007

[3] Gaudiosi D M, Reagan B, Popmintchev T, Grisham M, Berrill M, Cohen O, Walker B C, Murnane M M, Kapteyn H C and Rocca J J 2006 *PHYSICAL REVIEW LETTERS* **96** ISSN 0031-9007

[4] Walker B, Sheehy B, Kulander K and DiMauro L 1996 *PHYSICAL REVIEW LETTERS* **77** 5031–5034 ISSN 0031-9007

[5] Ekanayake N, Luo S, Wen B L, Howard L E, Wells S J, Videtto M, Mancuso C, Stanev T, Condon Z, LeMar S, Camilo A D, Toth R, Crosby W B, Grugan P D, Decamp M F and Walker B C 2012 *PHYSICAL REVIEW A* **86** ISSN 1050-2947

[6] Chowdhury E and Walker B 2003 *JOURNAL OF THE OPTICAL SOCIETY OF AMERICA B-OPTICAL PHYSICS* **20** 109–112 ISSN 0740-3224

[7] Ekanayake N, Luo S, Grugan P D, Crosby W B, Camilo A D, McCowan C V, Scalzi R, Tramontozzi A, Howard L E, Wells S J, Mancuso C, Stanev T, Decamp M F and Walker B C 2013 *PHYSICAL REVIEW LETTERS* **110** ISSN 0031-9007

[8] Corkum P 1993 *PHYSICAL REVIEW LETTERS* **71** 1994–1997 ISSN 0031-9007

[9] Yang B, Schafer K, Walker B, Kulander K, DiMauro L and Agostini P 1994 *ACTA PHYSICA POLONICA A* **86** 41–50 ISSN 0587-4246 international Conference on Quantum Optics III, SZCZYRK, POLAND, SEP 03-09, 1993

[10] Strickland D and Mourou G 1985 *OPTICS COMMUNICATIONS* **56** 219–221 ISSN 0030-4018

[11] Yoon J W, Kim Y G, Choi I W, Sung J H, Lee H W, Lee S K and Nam C H 2021 *OPTICA* **8** 630–635 ISSN 2334-2536

[12] Walser M, Keitel C, Scrinzi A and Brabec T 2000 *PHYSICAL REVIEW LETTERS* **85** 5082–5085 ISSN 0031-9007

[13] Palaniyappan S, Ghebregziabher I, DiChiara A, MacDonald J and Walker B C 2006 *PHYSICAL REVIEW A* **74** ISSN 1050-2947

[14] Chowdhury E, Ghebregziabiher I and Walker B 2005 *JOURNAL OF PHYSICS B-ATOMIC MOLECULAR AND OPTICAL PHYSICS* **38** 517–524 ISSN 0953-4075

[15] Ghebregziabher I and Walker B C 2007 *PHYSICAL REVIEW A* **76** ISSN 1050-2947

[16] Chowdhury E, Ghebregziabher I, MacDonald J and Walker B 2004 *OPTICS EXPRESS* **12** 3911–3920 ISSN 1094-4087

[17] Jones E, Germain Z, Niessner J, Milliken D, Scilla J, Kelley L, MacDonald J and Walker B C 2021 *PHYSICAL REVIEW A* **103** ISSN 2469-9926

[18] Palaniyappan S, DiChiara A, Chowdhury E, Falkowski A, Ongadi G, Huskins E and Walker B 2005 *PHYSICAL REVIEW LETTERS* **94** ISSN 0031-9007

[19] Kelley L, Germain Z, Jones E C, Milliken D and Walker B C 2021 *JOURNAL OF THE OPTICAL SOCIETY OF AMERICA B-OPTICAL PHYSICS* **38** 3646–3651 ISSN 0740-3224
[20] Klaiber M, Hatsagortsyan K Z, Wu J, Luo S S, Grugan P and Walker B C 2017 *PHYSICAL REVIEW LETTERS* **118** ISSN 0031-9007
[21] DiChiara A, Chowdhury E, Ongadi G, Walker B and Tamosaitis R 2003 *OPTICS LETTERS* **28** 2106–2108 ISSN 0146-9592
[22] Walker B, Toth C, Fittinghoff D, Guo T, Kim D, Rose-Petruck C, Squier J, Yamakawa K, Wilson K and Barty C 1999 *OPTICS EXPRESS* **5** 196–202 ISSN 1094-4087
[23] Perry M, Pennington D, Stuart B, Tietbohl G, Britten J, Brown C, Herman S, Golick B, Kartz M, Miller J, Powell H, Vergino M and Yanovsky V 1999 *OPTICS LETTERS* **24** 160–162 ISSN 0146-9592
[24] Chowdhury E, Barty C and Walker B 2001 *PHYSICAL REVIEW A* **63** ISSN 1050-2947
[25] Palaniyappan S, Mitchell R, Sauer R, Ghebregziabher I, White S L, Decamp M F and Walker B C 2008 *PHYSICAL REVIEW LETTERS* **100** ISSN 0031-9007
[26] Ekanayake N, Luo S, Grugan P D, Crosby W B, Camilo A D, McCowan C V, Scalzi R, Tramontozzi A, Howard L E, Wells S J, Mancuso C, Stanev T, Decamp M F and Walker B C 2013 *PHYSICAL REVIEW LETTERS* **110** ISSN 0031-9007
[27] Palaniyappan S, DiChiara A, Ghebregziabher I, Huskins E L, Falkowski A, Pajerowski D and Walker B C 2006 *JOURNAL OF PHYSICS B-ATOMIC MOLECULAR AND OPTICAL PHYSICS* **39** S357–S369 ISSN 0953-4075 10th International Conference on Multiphoton Processes (ICOMP 2005), Orford, CANADA, OCT 09-14, 2005
[28] DiChiara A D, Ghebregziabher I, Sauer R, Waesche J, Palaniyappan S, Wen B L and Walker B C 2008 *PHYSICAL REVIEW LETTERS* **101** ISSN 0031-9007
[29] Kornev A S, Tulenko E B and Zon B A 2011 *PHYSICAL REVIEW A* **84** ISSN 1050-2947
[30] Jones E C, Andreula Z P and Walker B C 2023 *PHYSICAL REVIEW A* **107** ISSN 2469-9926
[31] Salvat F, Jablonski A and Powell C 2005 *COMPUTER PHYSICS COMMUNICATIONS* **165** 157–190 ISSN 0010-4655
[32] Izaac J and Wang J 2018 *Computational Quantum Mechanics* (Springer Cham)
[33] Kramida A, Yu Ralchenko, Reader J and and NIST ASD Team 2021 NIST Atomic Spectra Database (ver. 5.9), [Online]. Available: `https://physics.nist.gov/asd` [2022, August 15]. National Institute of Standards and Technology, Gaithersburg, MD.
[34] Zettili N 2009 *Quantum Mechanics: Concepts and Applications* (Wiley) ISBN 9780470026786 URL `https://books.google.com/books?id=6jXlpJCSz98C`
[35] Ammosov M V 1987 *Sov. Phys. JETP* **64** 1191
[36] Frisch M J, Trucks G W, Schlegel H B, Scuseria G E, Robb M A, Cheeseman J R, Scalmani G, Barone V, Petersson G A, Nakatsuji H, Li X, Caricato M, Marenich A V, Bloino J, Janesko B G, Gomperts R, Mennucci B, Hratchian H P, Ortiz J V, Izmaylov A F, Sonnenberg J L, Williams-Young D, Ding F, Lipparini F, Egidi F, Goings J, Peng B, Petrone A, Henderson T, Ranasinghe D, Zakrzewski V G, Gao J, Rega N, Zheng G, Liang W, Hada M, Ehara M, Toyota K, Fukuda R, Hasegawa J, Ishida M, Nakajima T, Honda Y, Kitao O, Nakai H, Vreven T, Throssell K, Montgomery Jr J A, Peralta J E, Ogliaro F, Bearpark M J, Heyd J J, Brothers E N, Kudin K N, Staroverov V N, Keith T A, Kobayashi R, Normand J, Raghavachari K, Rendell A P, Burant J C, Iyengar S S, Tomasi J, Cossi M, Millam J M, Klene M, Adamo C, Cammi R, Ochterski J W, Martin R L, Morokuma K, Farkas O, Foresman J B and Fox D J 2016 Gaussian˜16 Revision C.01 gaussian Inc. Wallingford CT
[37] Grugan P D, Luo S, Videtto M, Mancuso C and Walker B C 2012 *PHYSICAL REVIEW A* **85** ISSN 1050-2947
[38] Bauke H, Hetzheim H G, Mocken G R, Ruf M and Keitel C H 2011 *PHYSICAL REVIEW A* **83** ISSN 2469-9926
[39] Peatross J, Mueller C and Keitel C H 2007 *OPTICS EXPRESS* **15** 6053–6061 ISSN 1094-4087
[40] Klaiber M, Yakaboylu E, Bauke H, Hatsagortsyan K Z and Keitel C H 2013 *PHYSICAL REVIEW LETTERS* **110** ISSN 0031-9007
[41] Milosevic N, Krainov V and Brabec T 2002 *JOURNAL OF PHYSICS B-ATOMIC MOLECULAR AND OPTICAL PHYSICS* **35** 3515–3529 ISSN 0953-4075
[42] Klaiber M, Hatsagortsyan K Z and Keitel C H 2007 *PHYSICAL REVIEW A* **75** ISSN 1050-2947
[43] Luo S S, Grugan P D and Walker B C 2014 *JOURNAL OF PHYSICS B-ATOMIC MOLECULAR AND OPTICAL PHYSICS* **47** ISSN 0953-4075